LARGE DEFLECTION MODEL: MULTI-DISK ROTATING SYSTEM

5.1 Introduction

Most machines are composed of many disks on the shaft periphery. The examples are blades in gas turbines/steam turbines. The multiple cams on the camshaft in a multi-cylinder engine (Automobile, Ships, and Power Plants). These multidisc systems are complex structures and difficult to analyze their vibration behavior. The presence of additional disks may alter the dynamics of the whole system. Therefore, it is inevitable to study the vibration analysis before putting them into working conditions for the proper functioning of the system.

In this section, mathematical formulation of a multiple disk rotating system with a harmonic base motion is carried out. The work of previous section is extended by considering multiple disks along the shaft length with rigid bearing support. The shaft is simply supported using rigid bearings so the boundary conditions corresponding to the simply supporting rigid bearings are considered.

5.2 Mathematical modeling

Figure 5.1 describes a flexible rotating shaft mounting multiple disks at various locations along the span subjected to a base motion. Here, the rotating system which includes a flexible shaft of length L, shaft mass m, four rigid-disk of outer radius R_d, disk mass M, the disk thickness h and simply supported to rigid bearing while rigid disks are here located at equal spacing. Coordinate system X-Y-Z is fixed at the left end of the shaft with X direction along the shaft length
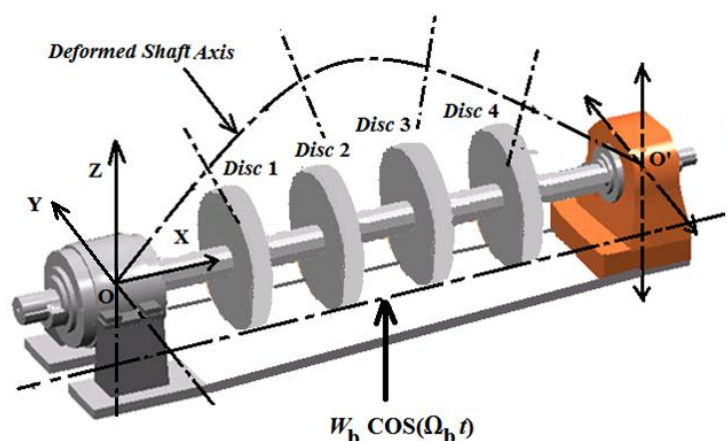

Fig.5.1: A rotating system model with multiple disks

The shaft bears multiple disk with equal space distribution along its length and the system is excited by harmonic base motion $\{W_b\cos(\Omega_b t)\}$. Thus, the Eqs.(4.1) and (4.2) (i.e. Kinetic energy of the system) can be redefined as below to include the effect of the multiple disks and the harmonic base motion.

$$T = \int_0^L \left(m(u_t^2 + v_t^2 + (w_t + W_b \cos(\Omega_b t))^2 + I_1 \omega_1^2 + I_2(\omega_2^2 + \omega_3^2)) \right) dx$$

$$+ \int_0^L \left(\sum_{n=1}^N M_n(u_t^2 + v_t^2 + (w_t + W_b \cos(\Omega_b t))^2 + \sum_{n=1}^N I_{1d_n} \omega_1^2 + \sum_{n=1}^N I_{2d_n}(\omega_2^2 + \omega_3^2)) \right) \Bigg|_{x=L_d} dx.$$

(5.1)

Here N, M_n, I_{1dn}, I_{2dn} represent total number of disks, mass, polar M.I. and diametrical M.I. of nth disk respectively. Using similar procedure as described in the chapter 4 and putting additional dimensionless parameters such as $\beta_{1_n} = M_n / mL$, $W_b^* = W_b / L$ into Eqs. (4.9) and (4.10),one may reconstruct the equations of motion towards non-dimensional form of the governing equations and associated boundary conditions for lateral vibration of the rotating shaft to include the effect of the multiple disks and the base motion as below

$$v_{tt} + v_{xx} \int_1^x \int_0^x (v_{xt}^2 + v_{xtt} v_x + w_{xt}^2 + w_{xtt} w_x) dx dx + v_x \int_0^x (v_{xt}^2 + v_{xtt} v_x + w_{xt}^2 + w_{xtt} w_x) dx) - I_2(2\Omega w_{xxt}$$

$$+ v_{xxtt}) + cv_t + (v_x^2 v_{xxxx} + v_x w_x w_{xxxx} + 3v_x w_{xx} w_{xxx} + v_{xx} w_{xx}^2 + v_x^3 + v_{xxxx} + w_x v_{xx} w_{xxx} + 4v_x v_{xx} v_{xxx})$$

$$- \sum_{n=1}^N I_{2d_n}(2\Omega w_{xxt} + v_{xxtt})\Big|_{x=L_{d_n}} + \sum_{n=1}^N \beta_{1n} \left(v_{tt} + v_{xx} \int_1^x \int_0^x (v_{xt}^2 + v_{xtt} v_x + w_{xt}^2 + w_{xtt} w_x) dx dx \right)\Bigg|_{x=L_{d_n}}$$

$$+ \sum_{n=1}^N \beta_{1n} (v_x \int_0^x (v_{xt}^2 + v_{xtt} v_x + w_{xt}^2 + w_{xtt} w_x) dx))\Big|_{x=L_{d_n}} = 0.$$

(5.2)

$$w_{tt} + w_{xx} \int_1^x \int_0^x (v_{xt}^2 + v_{xtt} v_x + w_{xt}^2 + w_{xtt} w_x) dx dx + w_x \int_0^x (v_{xt}^2 + v_{xtt} v_x + w_{xt}^2 + w_{xtt} w_x) dx + I_2(2\Omega v_{xxt}$$

$$- w_{xxtt}) + cw_t + (w_x^2 w_{xxxx} + w_x v_x v_{xxxx} + 3w_x v_{xx} v_{xxx} + w_{xx} v_{xx}^2 + w_{xx}^3 + w_{xxxx} + v_x w_{xx} v_{xxx} + 4w_x w_{xx} w_{xxx})$$

$$+ \sum_{n=1}^N I_{2d_n}(2\Omega v_{xxt} - w_{xxtt})\Big|_{x=L_{d_n}} + \sum_{n=1}^N \beta_{1_n} \left(w_{tt} + w_{xx} \int_1^x \int_0^x (v_{xt}^2 + v_{xtt} v_x + w_{xt}^2 + w_{xtt} w_x) dx dx \right)\Bigg|_{x=L_d}$$

$$+ \sum_{n=1}^N \beta_{1_n} (w_x \int_0^x (v_{xt}^2 + v_{xtt} v_x + w_{xt}^2 + w_{xtt} w_x) dx)\Big|_{x=L_{d_n}} = (1 + \sum_{n=1}^N \beta_{1_n}) W_b \Omega_b^2 \cos \Omega_b t.$$

(5.3)

Associated boundary conditions:

At x = 0, $v_{xx} = 0$, $v_{xxx} = 0$, $w_{xx} = 0$, $w_{xxx} = 0$.

At x = 1, $v_{xx} = 0$, $v_{xxx} = 0$, $w_{xx} = 0$, $w_{xxx} = 0$.

(5.4)

The partial differential equations i.e., Eqs.(5.2)-(5.3)) have been discretized using Galerkin's method by considering fundamental mode of vibration as single mode Galerkin's solution. Therefore, displacements fields (v, w) is being expressed as $v(x,t) = \varphi(x) R(t)$, and $w(x,t) = \varphi(x) S(t)$. Here, $\varphi(x)$ is the linear eigenfunction of a beam with simply supported and it is expressed as $\varphi(x) = \sqrt{2} \sin(\pi x)$. It satisfies the above boundary conditions (a set of algebraic equations). Substituting $\varphi(x)$ into the equations of motion (i.e. Eqs (5.2) -(5.3) for the rotating shaft, it results into the following equations

$$\kappa_1 R_{tt} + c\kappa_2 R_t + \kappa_3 R - 2\Omega \kappa_4 S_t + \kappa_5(R^3 + RS^2) + \kappa_7(RR_t^2 + RS_t^2 + R^2 R_{tt} + RSS_{tt}) = 0.$$

(5.5)

$$\kappa_1 S_{tt} + c\kappa_2 S_t + \kappa_3 S + 2\Omega \kappa_4 R_t + \kappa_5(S^3 + R^2 S) + \kappa_7(SR_t^2 + SS_t^2 + RSR_{tt} + S^2 S_{tt}) = \Upsilon \Omega_b^2 \cos \Omega_b t.$$

(5.6)

Here, the coefficients indicated in the above equations are being expressed below

$$\kappa_1 = \int_0^1 \left(\varphi^2 - \varphi \varphi'' I_2 + \sum_{n=1}^N (\varphi_{x=L_{d_n}}^2 \beta_{1_n} - \varphi_{x=L_{d_n}} (\varphi'')_{x=L_{d_n}} I_{2d_n}) \right) dx, \quad \kappa_2 = \int_0^1 (\varphi^2 + \varphi_{x=0}^2 + \varphi_{x=L}^2) dx,$$

$$\kappa_3 = \int_0^1 (\varphi \varphi'''' + \varphi_{x=0}^2 K_l + \varphi_{x=L}^2 K_l) dx, \quad \kappa_4 = \int_0^1 \left(\varphi \varphi'' I_2 + \sum_{n=1}^N (\varphi_{x=L_{d_n}} (\varphi'')_{x=L_{d_n}} I_{2d_n}) \right) dx,$$

$$\kappa_5 = \int_0^1 (\varphi \varphi'^2 \varphi'''' + \varphi \varphi''^3 + 4\varphi \varphi' \varphi'' \varphi''') dx, \quad \kappa_7 = \int_0^1 (\varphi \varphi'' \int_1^x \int_0^x \varphi'^2 dx dx + \sum_{n=1}^N \beta_{1_n} (\varphi \varphi'' \int_1^x \int_0^x \varphi'^2 dx dx)_{x=L_{d_n}}$$

$$+(\varphi\varphi'\int_0^x \varphi'^2 dx + \sum_{n=1}^N \beta_{1_n}(\varphi\varphi'\int_0^x \varphi'^2 dx)_{x=L_{d_n}}))dx, \quad c = \int_0^1 (\varphi^2 c)dx,$$

$$\Upsilon = W_b \int_0^1 (\varphi + \sum_{n=1}^N (\varphi_{d_n}\beta_{1_n})|_{x=L_{d_n}})dx.$$

It is quite evident that the above governing equations have nonlinear terms in the form of an external excitation and structural nonlinearities. Hence, approximate solutions are inevitable and required to be obtained by using similar procedure of the method of multiple scales as expressed in chapter 3 and 4. Then, we obtained the following expressions for order 1 of ε.

$$\kappa_1 D_0^2 R_3 + \kappa_3 R_3 - 2\Omega\kappa_4 D_0 S_3 =$$

$$\{2i(\kappa_4\Omega + \kappa_1 N_f)D_2 F_1(T_2) - i\kappa_2 c N_f F_1(T_2) - 4i\kappa_5 F_1^2\overline{F}_1 + (2\kappa_7(N_f+N_b)^2 - 8\kappa_5 F_1 F_2\overline{F}_2\}e^{N_f T_0 i} +$$

$$\{-2(\kappa_4\Omega - \kappa_1 N_b)D_2 F_2(T_2) - \kappa_2 c N_b F_2(T_2) - 4i\kappa_5 F_2^2\overline{F}_2 - (2\kappa_7(N_f+N_b)^2 - 8i\kappa_5 F_1 F_2\overline{F}_1\}e^{N_b T_0 i}$$

$$+CC + NST. \tag{5.7}$$

$$\kappa_1 D_0^2 S_3 + \kappa_3 S_3 + 2\Omega\kappa_4 D_0 R_3 =$$

$$\begin{cases} \dfrac{1}{2}\Upsilon\Omega_b^2 e^{i\sigma T_0} - 2(\kappa_4\Omega + \kappa_1 N_f)D_2 F_1(T_2) + \kappa_2 c N_f F_1(T_2) - 4i\kappa_5 F_1^2\overline{F}_1 \\ +i(2(\kappa_7 + \kappa_{7d})(N_f+N_b)^2 + 8\kappa_5 F_1 F_2\overline{F}_2 \end{cases} e^{N_f T_0 i} +$$

$$\begin{cases} -2(\kappa_4\Omega + \kappa_1 N_b)D_2 F_2(T_2) - \kappa_2 c N_b F_2(T_2) - 4i\kappa_5 F_2^2\overline{F}_2 \\ +i(2\kappa_7(N_f+N_b)^2 - 8\kappa_5)F_1 F_2\overline{F}_1 \end{cases} e^{N_b T_0 i} + CC + NST. \tag{5.8}$$

Above equations are non-homogeneous equations that lead to secular or small divisor terms when the excitation frequency matches with forward natural frequency as $\Omega_b = N_f + \varepsilon^2\sigma$ called as primary resonance condition. As a result, the solutions from these equations may lead into unbounded solutions. Therefore, it is necessary to satisfy the certain solvability conditions prior to determine the bounded steady state solutions. We can obtain the following solvability conditions as.

$$\dfrac{1}{2}\Upsilon\Omega_b^2 e^{i\sigma T_0} - 2(\kappa_4\Omega + \kappa_1 N_f)D_2 F_1(T_2) + \kappa_2 c N_f F_1(T_2) - 4i\kappa_5 F_1^2\overline{F}_1$$

$$+i(2(\kappa_7 + \kappa_{7d})(N_f+N_b)^2 + 8\kappa_5)F_1 F_2\overline{F} = 0. \tag{5.9}$$

$$2(\kappa_4\Omega + \kappa_1 N_b)D_2 F_2(T_2) - \kappa_2 c N_b F_2(T_2) - 4i\kappa_5 F_2^2\overline{F}_2 + i(2\kappa_7(N_f+N_b)^2 - 8\kappa_5)F_1 F_2\overline{F}_1 = 0. \tag{5.10}$$

Expressing F_1 and F_2 in the polar forms $(1/2)a_1 e^{i\theta_1}$ and $(1/2)a_2 e^{i\theta_2}$, respectively and substituting into the above equations. We can obtain following expressions by collecting the real and imaginary terms separately.

$$\theta' = -\dfrac{(2N_f^2 k_7 - k_5)a_2^2}{(\Omega k_4 + N_f k_1)} - \dfrac{(N_f^2 k_7 - k_5/2)a_1^2}{(\Omega k_4 + N_f k_1)} - \dfrac{\Upsilon\Omega_b^2 \sin(\gamma)}{2a_1(\Omega k_4 + N_f k_1)}. \tag{5.11}$$

$$a_1' = -\dfrac{(N_f ck_2/2)a_1}{(\Omega k_4 + \omega_1 k_1)} - \dfrac{\Upsilon\Omega_b^2 \cos(\gamma)}{2(\Omega k_4 + N_f k_1)}. \tag{5.12}$$

$$\dfrac{\partial\gamma}{\partial T_2} = \sigma - \dfrac{\partial\theta_1}{\partial T_2}. \tag{5.13}$$

Eqs.(5.12) and (5.13) can be set to zero i.e., $a_1' = \gamma' = 0$ for obtaining the steady-state solution for a primary resonance condition. As a result, a set of nonlinear algebraic equations are obtained and it can be numerically solved to determine the amplitude of response d_1 for a change in values of the system parameters.

5.3 Viscoelastic shaft with base excitation

One of the causes of the nonlinearities is due to large elastic deformation. The use of damping in such system can be helpful to attenuate the large deformation and consequently reduce the severity of the nonlinear effects. Viscoelastic material has good damping property and is being widely used to passively control the vibration. The researchers such as Roy et al. (2016, 2017), Deng et al. (2016), Ganguly et al. (2016) did recently dynamic analysis of the viscoelastic rotating system. They used a viscoelastic material for the rotor in their's analysis. Here, we use a viscoelastic material instead of elastic one for the purpose of reducing the level of vibration in the modern development of rotating systems.

5.3.1 Analysis

Similar model of a multidisc rotating system (Fig.5.1) is considered here with the effect of a viscoelastic material for the shaft. Young modulus (E^*) of viscoelastic shaft is represented by complex quantity $E_1 + iE_2 = E_1(1 + iE_2/E_1) = E_1(1+i\delta)$ [Barun et al, 2008]. The E_1 represents elastic behavior and E_2 represents viscous behavior of the material. The δ is loss factor and it represents energy dissipative property of the material. The shaft carries multiple disks with equal space distribution along its length and the system is excited by a harmonic base motion ($W_b\cos(\Omega_b t)$). The expressions for the kinetic and potential energy of the system are described earlier in the previous section and chapter 4. The viscoelastic effect is included in the system by using E^* of the viscoelastic material in deriving the potential energy of the system. Thus, the equations of motion (i.e. Eqs.(5.2)-(5.3)) for the system become

$$v_{tt} + v_{xx}\int_1^x\int_0^x (v_{xt}^2 + v_{xtt}v_x + w_{xt}^2 + w_{xtt}w_x)dxdx + v_x\int_0^x (v_{xt}^2 + v_{xtt}v_x + w_{xt}^2 + w_{xtt}w_x)dx) - I_2(2\Omega w_{xxt}$$
$$+v_{xxtt})_t + (1+i\delta)(v_x^2 v_{xxxx} + v_x w_x w_{xxxx} + 3v_x w_{xx}w_{xxx} + v_{xx}w_{xx}^2 + v_x^3 + v_{xxxx} + w_x v_{xx}w_{xxx} + 4v_x v_{xx}v_{xxx})$$
$$-\sum_{n=1}^N I_{2d_n}(2\Omega w_{xxt} + v_{xxtt})\Big|_{x=L_{d_n}} + \sum_{n=1}^N \beta_{1n}\left(v_{tt} + v_{xx}\int_1^x\int_0^x (v_{xt}^2 + v_{xtt}v_x + w_{xt}^2 + w_{xtt}w_x)dxdx\right)\Big|_{x=L_{d_n}}$$
$$+cv_t + \sum_{n=1}^N \beta_{1n}(v_x\int_0^x (v_{xt}^2 + v_{xtt}v_x + w_{xt}^2 + w_{xtt}w_x)dx)dx)\Big|_{x=L_{d_n}} = 0. \tag{5.14}$$

$$w_{tt} + w_{xx}\int_1^x\int_0^x (v_{xt}^2 + v_{xtt}v_x + w_{xt}^2 + w_{xtt}w_x)dxdx + w_x\int_0^x (v_{xt}^2 + v_{xtt}v_x + w_{xt}^2 + w_{xtt}w_x)dx + I_2(2\Omega v_{xxt}$$
$$-w_{xxtt}) + (1+i\delta)(w_x^2 w_{xxxx} + w_x v_x v_{xxxx} + 3w_x v_{xx}v_{xxx} + w_{xx}v_{xx}^2 + w_{xx}^3 + w_{xxxx} + v_x w_{xx}v_{xxx} + 4w_x w_{xx}w_{xxx})$$
$$+\sum_{n=1}^N I_{2d_n}(2\Omega v_{xxt} - w_{xxtt})\Big|_{x=L_{d_n}} + \sum_{n=1}^N \beta_{1_n}\left(w_{tt} + w_{xx}\int_1^x\int_0^x (v_{xt}^2 + v_{xtt}v_x + w_{xt}^2 + w_{xtt}w_x)dxdx\right)\Big|_{x=L_d}$$
$$+cw_t + \sum_{n=1}^N \beta_{1_n}(w_x\int_0^x (v_{xt}^2 + v_{xtt}v_x + w_{xt}^2 + w_{xtt}w_x)dx)\Big|_{x=L_{d_n}} = (1+\sum_{n=1}^N \beta_{1_n})W_b\Omega_b^2\cos\Omega_b t. \tag{5.15}$$

Associated boundary conditions:

At x = 0, $v_{xx}=0, \quad v_{xxx}=0, \quad w_{xx}=0, \quad w_{xxx}=0.$

At $x=1$, $v_{xx}=0, \quad v_{xxx}=0, \quad w_{xx}=0, \quad w_{xxx}=0.$ \hfill (5.16)

Using the similar procedures and mathematical treatments on the above equation as per adopted in the previous sections, the equations of motion for the rotating shaft can be expressed as

$$\kappa_1 R_{tt} + c\kappa_2 R_t + (1+i\delta)\kappa_3 R - 2\Omega\kappa_4 S_t + \kappa_5(1+i\delta)(R^3 + RS^2) + \kappa_7(RR_t^2 + RS_t^2 + R^2 R_{tt} + RSS_{tt}) = 0. \tag{5.17}$$

$$\kappa_1 S_{tt} + c\kappa_2 S_t + \kappa_3(1+i\delta)S + 2\Omega\kappa_4 R_t + \kappa_5(1+i\delta)(S^3 + R^2 S) + \kappa_7(SR_t^2 + SS_t^2 + RSR_{tt} + S^2 S_{tt}) = \Upsilon\Omega_b^2\cos\Omega_b t. \tag{5.18}$$

Above governing equations exhibit complex and highly nonlinear in nature in terms of external excitation and structural nonlinearities. Hence, approximate solutions are inevitable and required to be obtained by using similar perturbation technique as chapter 3 and 4. We obtain the following expressions for order 1 of ε. .....

$$\kappa_1 D_0^2 R_3 + \kappa_3 R_3 - 2\Omega\kappa_4 D_0 S_3 =$$

$$\left\{ \begin{array}{l} 2i(\kappa_4\Omega + \kappa_1 N_f)D_2 F_1(T_2) - i\left(\kappa_2 c N_f + \delta\kappa_3\right)F_1(T_2) - \\ 4i((1+i\delta)\kappa_5)F_1^2\overline{F_1} + (2\kappa_7(N_f + N_b)^2 - 8((1+i\delta)\kappa_5))F_1 F_2\overline{F_2} \end{array} \right\} e^{N_f T_0 i} +$$

$$\left\{ \begin{array}{l} -2(\kappa_4\Omega - \kappa_1 N_b)D_2 F_2(T_2) - \left(\kappa_2 c N_b + \delta\kappa_3\right)F_2(T_2) - \\ 4i((1+i\delta)\kappa_5)F_2^2\overline{F_2} - (2\kappa_7(N_f + N_b)^2 - 8i((1+i\delta)\kappa_5))F_1 F_2\overline{F_1} \end{array} \right\} e^{N_b T_0 i} + CC + NST. \tag{5.19}$$

$$\kappa_1 D_0^2 S_3 + \kappa_3 S_3 + 2\Omega\kappa_4 D_0 R_3 =$$

$$\left\{ \begin{array}{l} \dfrac{1}{2}\Upsilon\Omega_b^2 e^{i\sigma T_0} - 2(\kappa_4\Omega + \kappa_1 N_f)D_2 F_1(T_2) + \left(\kappa_2 c N_f + \delta\kappa_3\right)F_1(T_2) - \\ 4i((1+i\delta)\kappa_5)F_1^2\overline{F_1} + i(2(\kappa_7 + \kappa_{7d})(N_f + N_b)^2 + 8((1+i\delta)\kappa_5))F_1 F_2\overline{F_2} \end{array} \right\} e^{N_f T_0 i} +$$

$$\left\{ \begin{array}{l} -2(\kappa_4\Omega + \kappa_1 N_b)D_2 F_2(T_2) - \left(\kappa_2 c N_b + \delta\kappa_3\right)F_2(T_2) - 4i\kappa_5 F_2^2\overline{F_2} + \\ i(2\kappa_7(N_f + N_b)^2 - 8\kappa_5)F_1 F_2\overline{F_1} \end{array} \right\} e^{N_b T_0 i} + CC + NST. \tag{5.20}$$

Here, the above non-homogeneous equations lead to secular or small divisor terms when the excitation frequency matches with forward natural frequency as $\Omega_b = N_f + \varepsilon^2\sigma$ called as a primary resonance condition. As a result, solutions from these equations may lead into unbounded solutions. Thus, we equate the secular parts to zero as a fundamental solubility condition to obtain the bounded solutions and it results in the following solvability conditions as.

$$\dfrac{1}{2}\Upsilon\Omega_b^2 e^{i\sigma T_0} - 2(\kappa_4\Omega + \kappa_1 N_f)D_2 F_1(T_2) + \left(\kappa_2 c N_f + \delta\kappa_3\right)F_1(T_2)$$
$$-4i(1+i\delta)\kappa_5 F_1^2\overline{F_1} + i(2(\kappa_7 + \kappa_{7d})(N_f + N_b)^2 + 8(1+i\delta)\kappa_5)F_1 F_2\overline{F} = 0. \tag{5.21}$$

$$2(\kappa_4\Omega + \kappa_1 N_b)D_2 F_2(T_2) - \left(\kappa_2 c N_b + \delta\kappa_3\right)F_2(T_2) - 4i\kappa_5 F_2^2\overline{F_2} +$$
$$i(2\kappa_7(N_f + N_b)^2 - 8\kappa_5)F_1 F_2\overline{F_1} = 0. \tag{5.22}$$

Expressing F_1 and F_2 in the polar forms $(1/2)a_1 e^{i\theta_1}$ and $(1/2)a_2 e^{i\theta_2}$, respectively and substituting into these solvability conditions (Eqs. (5.21) and (5.22)). We can obtain following expressions by collecting the real and imaginary terms separately.

$$\theta' = -\dfrac{\left(2N_f^2 k_7 - k_5\right)a_2^2}{\left(\Omega k_4 + N_f k_1\right)} - \dfrac{\left(N_f^2 k_7 - k_5/2\right)a_1^2}{\left(\Omega k_4 + N_f k_1\right)} - \dfrac{\Upsilon\Omega_b^2 \sin(t\sigma 1)}{2a_1\left(\Omega k_4 + N_f k_1\right)}. \tag{5.23}$$

$$a_1' = \dfrac{-k_5\delta a_1 a_2^2}{\left(\Omega k_4 + \omega_1 k_1\right)} - \dfrac{\delta k_5 a_1^3}{2\left(\Omega k_4 + \omega_1 k_1\right)} - \dfrac{\left(k_3\delta/2 + \omega_1 c k_2/2\right)a_1}{\left(\Omega k_4 + \omega_1 k_1\right)} - \dfrac{\Upsilon\Omega_b^2 \cos(t\sigma 1)}{2\left(\Omega k_4 + \omega_1 k_1\right)}. \tag{5.24}$$

$$\dfrac{\partial\gamma}{\partial T_2} = \sigma - \dfrac{\partial\theta_1}{\partial T_2}. \tag{5.25}$$

In these equations, we can be set $a_1' = \gamma' = 0$ for obtaining the steady-state solution for the primary resonance condition. As a result, a set of nonlinear algebraic equations are obtained and can be numerically solved to determine the amplitude of response d_1 for a change in values of system parameters.

5.3.2 Result and Discussion

For this numerical investigation, polymethyl methacrylate as a viscoelastic material is used for the shaft. The rotating system is considered with shaft length ($L = 0.6$ m), mass density 1190.2357 kg/m^3, young modulus $E_1 = 3\times10^9$ N/m^2, loss factor $\delta = 0.05$, disk diameter ($R_d = 0.07$ m), Non-dimensional disk mass ($\beta_1 = 1.2$), diametrical moment of inertia ($I_3 = 0.000625$) and base excitation magnitude ($W_b = 0.05$). Theoretical studies have been carried out to critically observe the stability, its state of evaluation and operating points under the primary resonance condition

when the parameters of the rotating shaft-disk system such as loss factor, no. of the disk, frequency, and magnitude of the base excitation, have been varied. These observations have been demonstrated using the frequency response characteristic, time responses, state-space solutions, and Poincare's tool to examine the vibration attributes of the system.

The effect of vibration characteristics by considering the multiple disks mounted on the shaft has been portrayed in Fig.5.2.With increase in the number of disks, the system losses its hardening behavior which in turns the response curves bent left and as a result, the maximum response amplitude is found to be significantly increased. However, the jump length is found to be almost same and hence, catastrophic failure due to the sudden change in the amplitude is almost trivial. The region of bi-stability gets expanded and the instability covers wide range of the excitation frequency as compared to the single-disc system. Therefore, initial operating condition plays a decisive factor indicating whether the system vibrates with large amplitude leading to the catastrophic failure. Here, understanding the basin of attraction might be helpful in accordance with the system stability while selecting the initial condition.
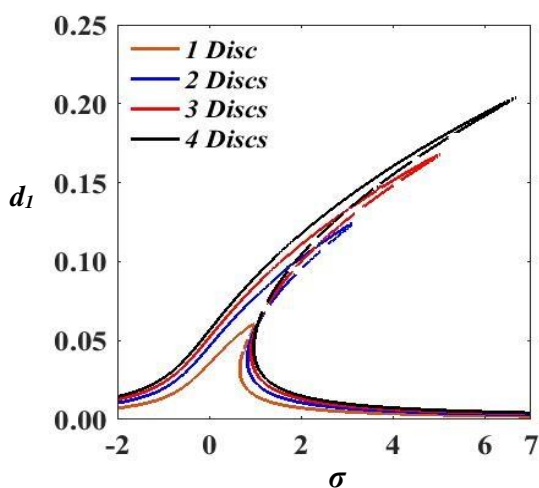
Fig.5.2: Frequency response curve for multiple disks
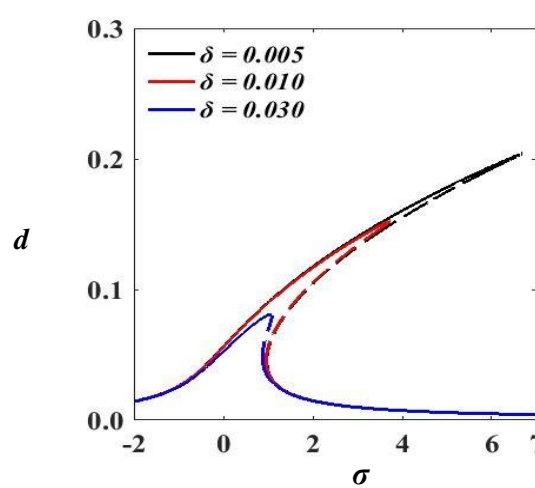
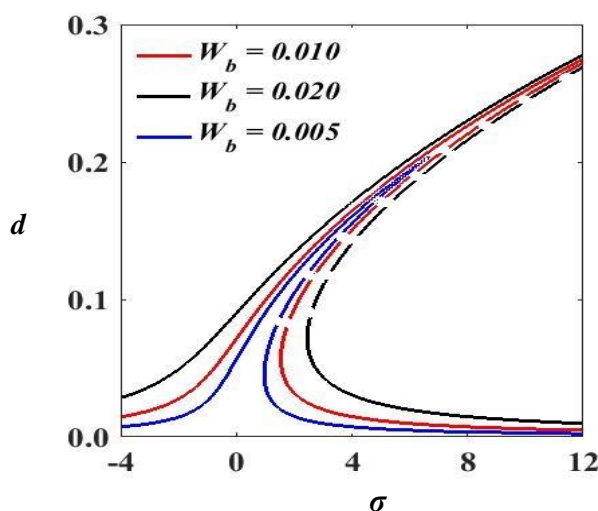**Fig.5.3:** Frequency response curve for different loss factor (δ)

Fig.5.4: Frequency response curve for different magnitude of the base excitation (W_b)

Figure 5.3 is demonstrated to show the effect of loss of factor accounting the viscous property δ on the dynamic behavior of the rotating system. It has been observed that introducing the high loss factor in the system causes decrease in the amplitude. The region of the instability gets disappeared with increase in the loss factor or for a system with high loss factor. Hence, the

system with high loss factor reduces the chances of catastrophic failure due to the non-existence of S-N bifurcation. Therefore, using viscoelastic material instead of elastic material one may attenuate the level of vibration and hence, the catastrophic failure

The effect of change in a magnitude of the base excitation (W_b) on the dynamic behavior of the system near the resonance condition is portrayed in Fig.5.4. The increasing the magnitude causes the increase in the vibration amplitude as well as increases the instability region. As a result, length of the jump up/down gets escalated which in turn increases the chances of catastrophic failure while the critical bifurcation starts at a higher frequency.
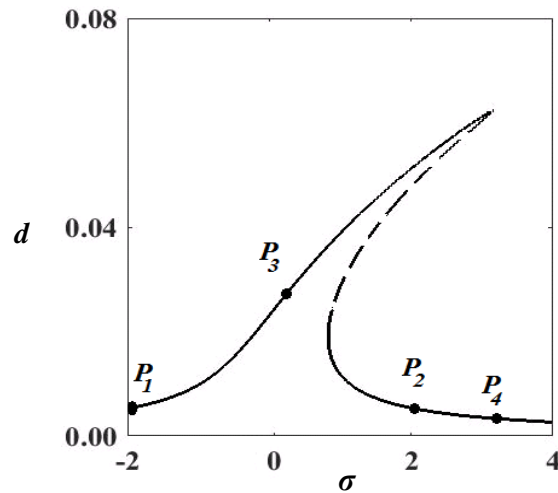
Fig.5.5: Frequency response curve

Figures 5.5- 5.6 are used to compare the results of the method of multiple scales with the findings obtained directly integrating the equation of motion. Figure 5.6 exhibits time histories, phase portrait and Poincare's section corresponding to points P_1, P_2. P_3 and P_4 marked in the frequency response curve (Fig.5.5). However, the both results are in a compliance and the system shows periodic behavior at all these points. A typical frequency response curves dealing the vibration amplitude with the external frequency of the base excitation leading a primary resonance condition has been depicted. Here, the solid and dotted lines indicate the stable and unstable solutions, respectively. As the system does not impart any trivial state response, the rotating shaft vibrates always with an amplitude equal to the non-trivial response as portrayed in Fig.5.5.
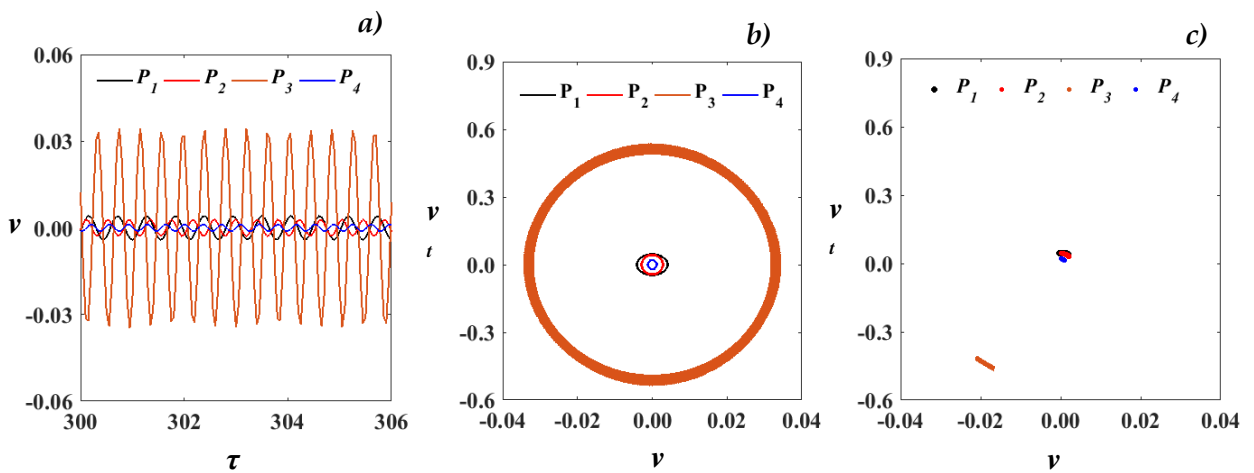

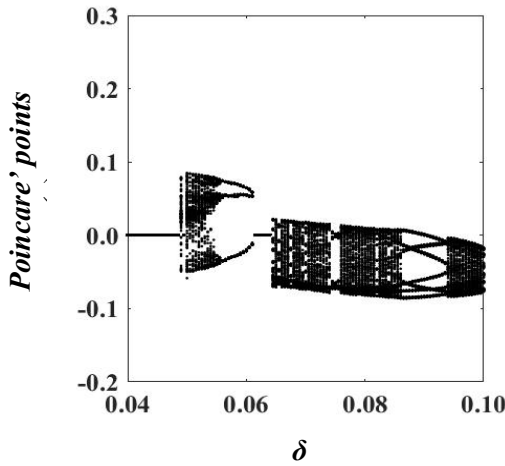**Fig.5.6:** a) Time series b) Phase portrait map c) Poincare' map (Ref. Fig.5.5)

Fig.5.7: Bifurcation diagram for effect of δ,N=4, Ω$_b$ =50,

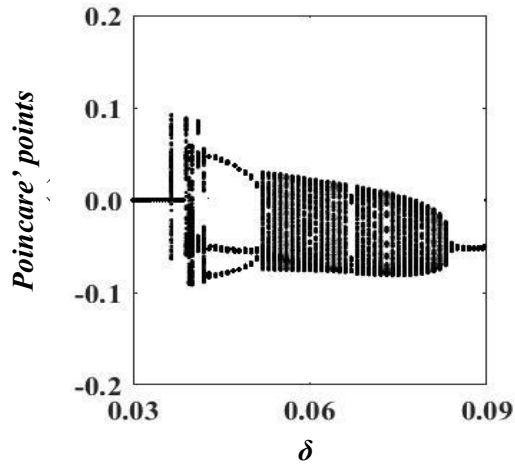**Fig.5.8:** Bifurcation diagram for effect of δ, N=2, Ω$_b$ =72,

The bifurcation diagrams are presented for the system with 4 disc and 2 discs in Fig.5.7 and Fig.5.8, respectively. The time response, phase portrait and Poincare's map are plotted corresponding to δ= 0.045, 0.052, 0.057, 0.080 in Fig.5.9 to analyze the system behavior at the various loss factor (δ) for the system with 4 discs. The bifurcation diagram for the system with 4 discs shows periodic behavior for δ<0.048 and 0.0615<δ<0.0645 and it is verified by observing the phase portrait and Poincare's map correspond to δ= 0.045 in Fig.5.9. The phase portraits of these responses show trajectories with a very small amplitudes as compared to others. Therefore, the Poincare's map shows almost a dot and this behavior can be neglected or assumed as a periodic behavior.
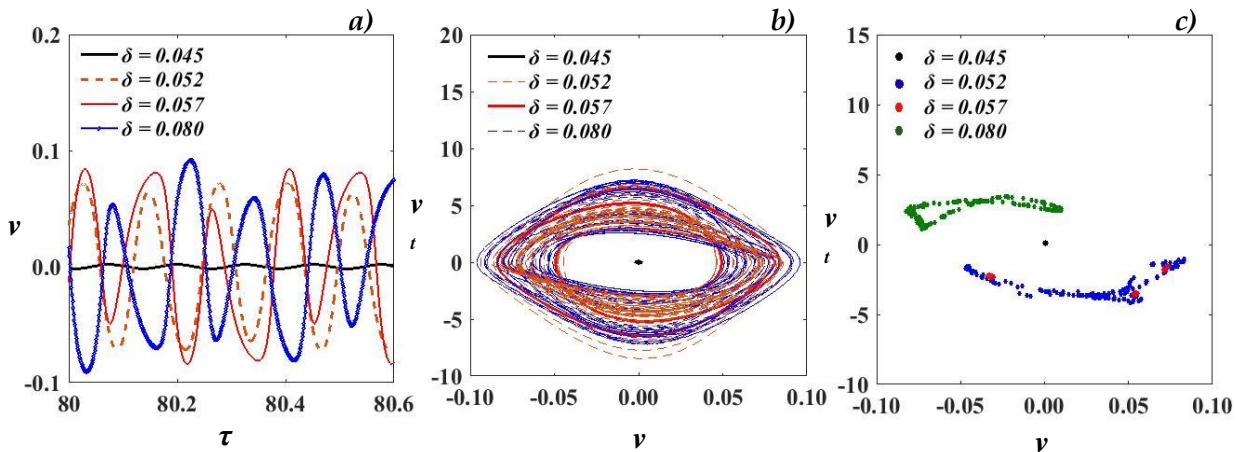

Fig.5.9: Effect of loss factor δ a) Time series b) Phase portrait map c) Poincare' map

When the δ is increased above 0.048, the system shows sudden change in its nature from a periodic behavior to a chaotic. The chaotic behavior is detected by developing the Poincare's map at δ=0.052 as shown in Fig.5.9. The scattered points on the Poincare's map is corresponds to unpredictable behavior of the system. At δ=0.057, the Poincare's map in Fig.5.9 shows system behavior with three periods. Further the increase in the δ causes the nature of the system to transform into a periodic behavior at δ=0.064. The Fig.5.7 shows quasiperiodic nature for 0.0640< δ<0.086 and δ> 0.0935, this can be detected using the Poincare's map in Fig.5.9 which is corresponding to δ=0.080 as the Poincare's map shows a closed curve. For the small range of δ from 0.0745 to 0.0755, the system shows multiperiodic behavior as well as it is also repeated for a range from 0.0865 to 0.0935. In this case, when the number of the disc is reduced to two, the system shows shifting the start of the chaotic region to lower value δ=0.0395 as compared to Fig.5.7. As well as the regions of the quasiperiodic and multiperiodic behaviour are squeezed to a

smaller range i.e., $0.0515 < \delta < 0.084$ such that the multiperiodic regions are almost vanished in Fig.5.8.
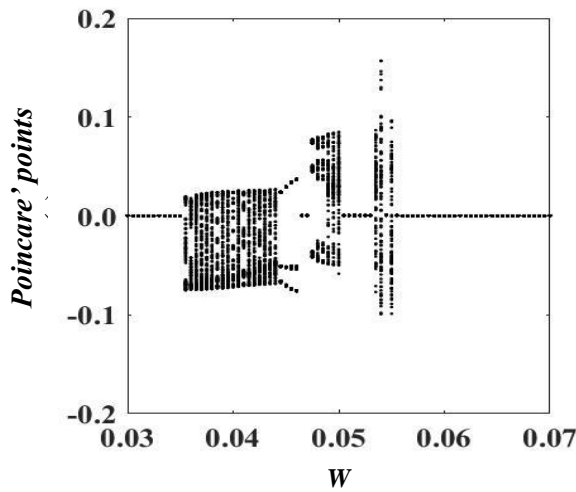

Fig.5.10: Bifurcation diagram for effect of W_b, N=4, Ω_b =50
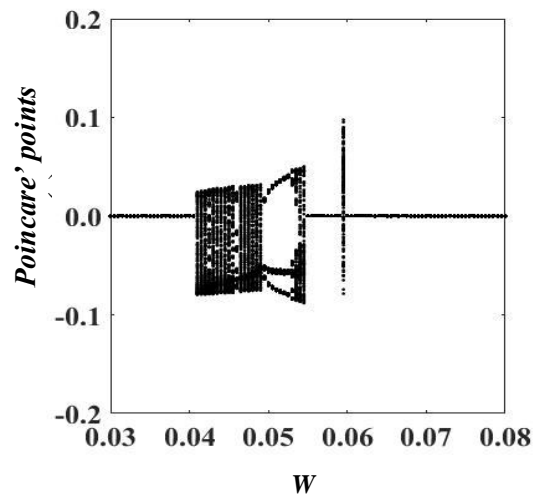
Fig.5.11: Bifurcation diagram for effect of W_b, N=2, Ω_b =72

Evolution of the system behavior due to change in the W_b is established in Figs.5.10 and 5.11 with 4 discs and 2 discs respectively. The horizontal straight line in the figures show a periodic behavior. In Fig.5.10, the system undergoes a periodic behavior till $W_b<0.035$, then it gets transformed to a quasi-periodic nature. When the value of W_b increased above the 0.045, the system vibrates with three times of the excitation frequency then it is subjected to double periodic transformation till $W_b = 0.05$ and the system exhibit a chaotic nature at this value. Then, it suddenly jumps to a periodic behavior for further increase in the W_b. A similar transformation of the system nature is also observed for the system with 2 Disc as shown in Fig.5.11 such as a periodic behavior for $W_b<0.041$ and $W_b>0.056$, quasi-periodic behaviour for $0.041< W_b<0.049$ and double periodic nature from $0.049<W_b<0.056$.
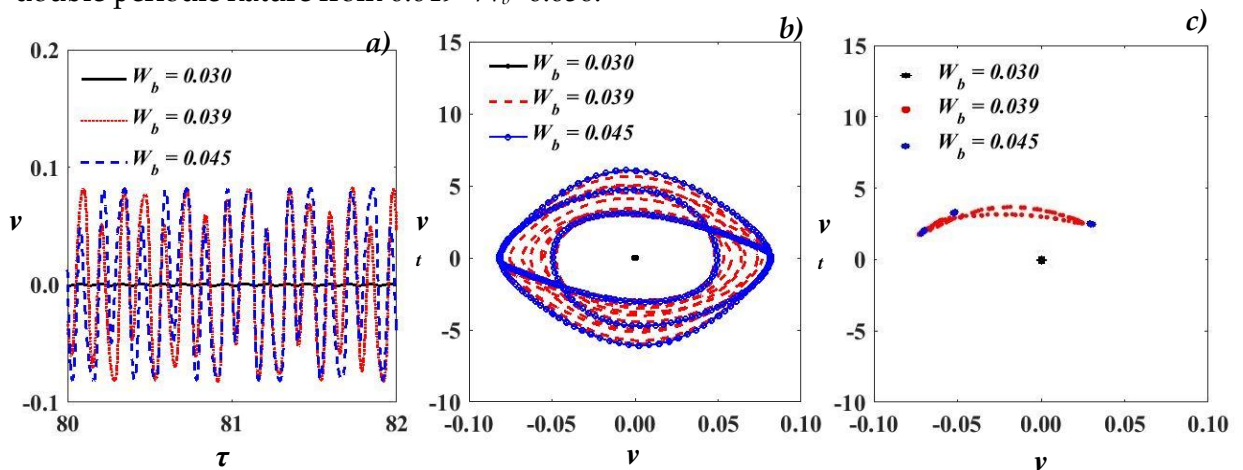
Fig.5.12: Effect of W_b a) Time series b) Phase portrait map c) Poincare' map

This transformation is verified by developing Fig.5.12 and Fig.5.13 for the system with 4 discs. The system shows a periodic, triple periodic and quasi-periodic nature at W_b =0.030, 0.039 and 0.045 respectively in Fig.5.12. And, a chaotic behaviour of the system is observed at W_b =0.05 in Fig.5.13. It has been observed that the similar transformation of the system behaviour can be observed in both these figures. But, the region of transformation from the periodic to the quasi-

periodic is shifted to a higher value of W_b (i.e W_b = 0.041) for the system with 2 discs than the 4 discs (i.e. W_b = 0.035) which is almost opposite as described for the effect of loss factor δ.
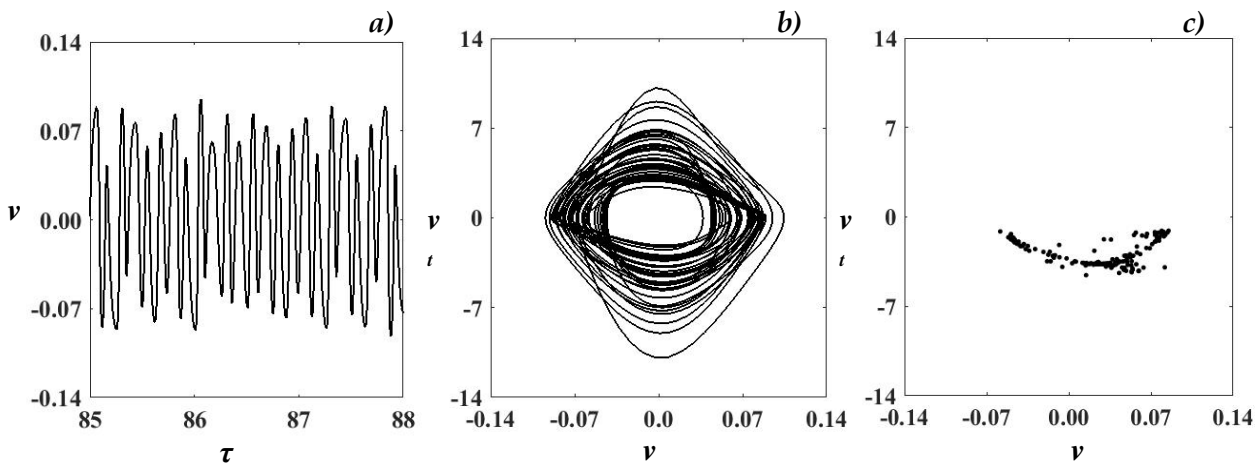

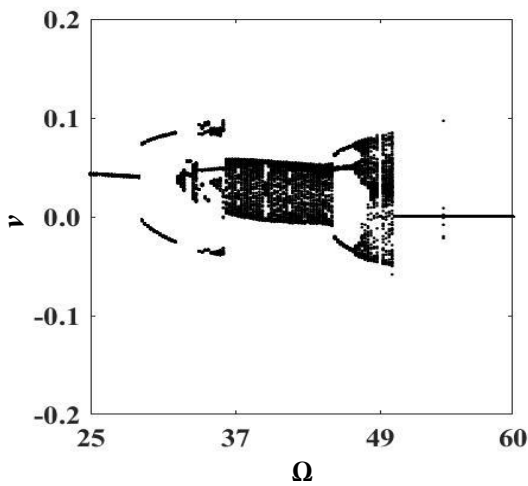**Fig.5.13:** Effect of W_b a) Time series b) Phase portrait mapc) Poincare' map (W_b = 0.05)

Fig.5.14: Bifurcation diagram for effect of Ω_b, N=4
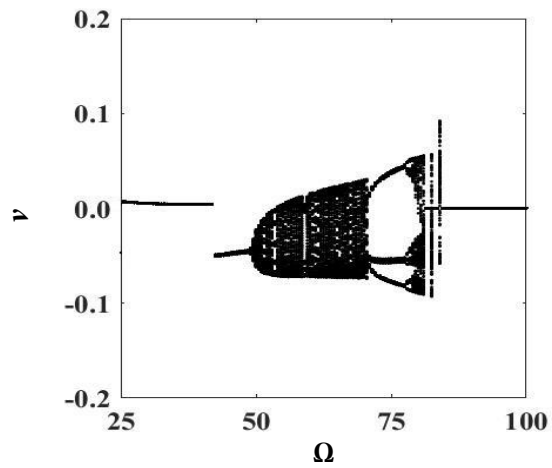
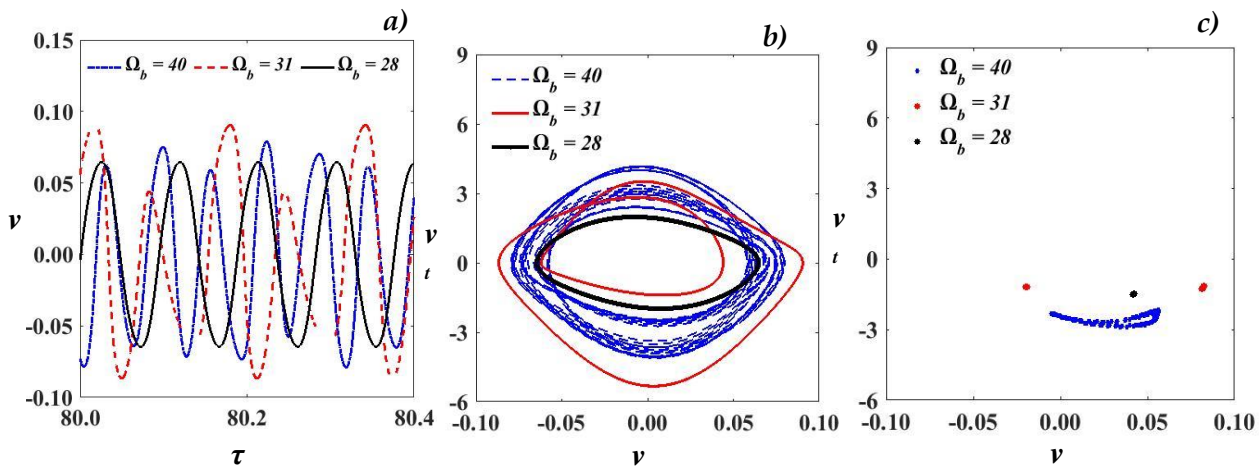**Fig.5.15:** Bifurcation diagram for effect of Ω_b, N=2

Fig.5.16: Effect of Ω_b a) Time series b) Phase portrait map c) Poincare' map

Figures 5.14-5.15 are bifurcation diagrams of the rotating systems with 4 disc and 2 disc, respectively to understand the evolutionary behavior of the system due to a change in Ω_b. In Fig.5.14, the system shows a periodic behavior for Ω_b< 29 and Ω_b> 50.2, quasi-periodic behavior for 36.25 <Ω_b< 45 and transformation to the chaotic nature when 29 <Ω_b < 36.25 and 45 <Ω_b <

50.25. This transformation is verified by developing Fig.5.16 and Fig.5.17 at Ω_b= 28, 31, 40 and 50. It has been verified that the system has a periodic, double periodic, quasi-periodic and chaotic nature respectively at these values of Ω_b. The region of bifurcation for the system with 4 discs is started at a lower value of the Ω_b as compared to the system with two discs but the bifurcation range is more in case of the system with 4 disks. The system behaviour shows two times the route to chaotic transformation for the 4 disks system as compared to the one-time evidence of the route to chaotic transformation in the case of two discs system.
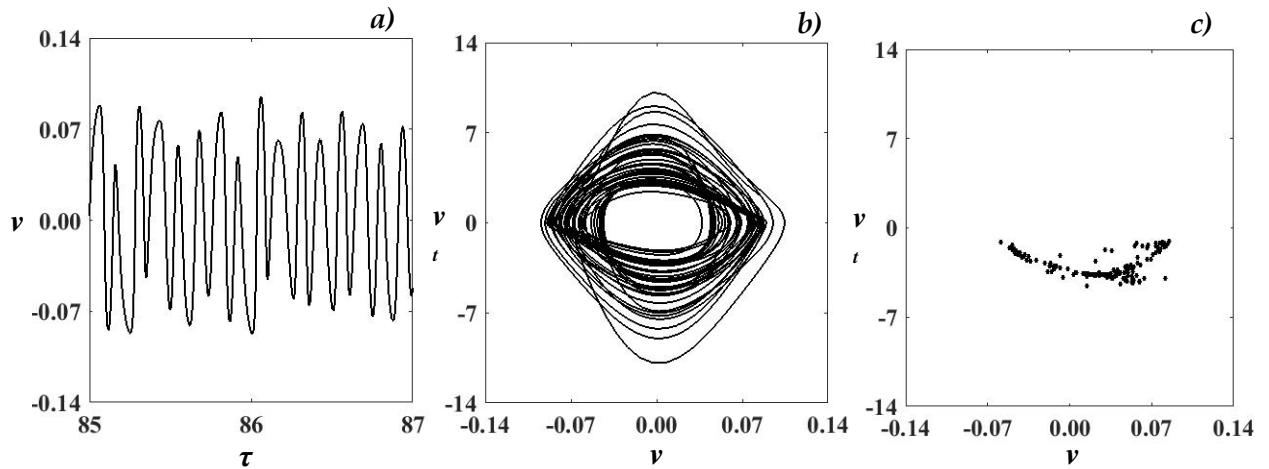

Fig.5.17: Effect of Ω_b a) Time series b) Phase portrait map c) Poincare' map (Ω_b= 50)

5.4 Summary

A mathematical model of the rotor system with multiple disks under the influence of an external excitation due to the base motion is formulated with the nonlinear curvature and gyroscopic effect. Further, a viscoelastic material for the shaft is used to analyze the effect of the material on nonlinear behavior of the system. A set of the nonlinear algebraic equations have been derived from the nonlinear differential governing equation using the method of multiple scales to further obtain the system responses and their stability.

The stability of the system near the resonance condition is analyzed by portraying the effect of no of disks, frequency and magnitude of the base excitation. As well as, the evolution of the system behavior (such as route to chaos) has been investigated using the bifurcation diagrams. The behavior of the system on the bifurcation diagrams has been verified at the different values using the time response plots, phase portrait plot and Poincare maps.

Based on the outcomes, the following observations have been depicted in the present work.

✔ The behavior of the system can be successfully controlled with an appropriate selection of base excitation frequency and magnitude as well as the possibility of instability and catastrophic failure of the system can also be attenuated.

✔ With increase in the number of disks causes the increase in the vibration amplitude and expansion of the instability region. The viscous material with sufficient loss factor can attenuate the vibration amplitude and decrease the instability region, consequently it decrease the severity of the catastrophic failure.

✔ The amplitude and the instability range get smaller for lower value of the base excitation parameters (such as W_b) and the other way around.

✔ Finally, the systems parameters (N, δ, Ω_b and W_b) strongly exhibit the presence of chaotic region when its value crosses to one of its critical value.

Outcomes from this work enable significant theoretical understanding of forced vibration analyses which are of great practical importance for investigating the dynamic performance.